Evidence for one-, two-, and three-dimensional order in a system of hard parallel spherocylinders

A. Stroobants and H. N. W. Lekkerkerker
Van 't Hoff Laboratorium, Rijksuniversiteit Utrecht, 3584 CH Utrecht, The Netherlands

D. Frenkel
Fysisch Laboratorium, Rijksuniversiteit Utrecht, 3508 TA Utrecht, The Netherlands
(Received 4 March 1987)

The phase diagram of a system of hard parallel spherocylinders with length-to-width ratios L/D between 0 and ∞ is investigated by Monte Carlo simulation. In addition to a low-density nematic phase and a high-density crystalline phase, two phases with partial translational order are observed, viz., a smectic phase and a columnar phase. By computing the absolute free energy of all phases, their range of stability and coexistence points are determined. For L/D ratios exceeding 0.5, a stable smectic phase is formed at densities well below the thermodynamic melting point. The nematic-to-smectic transition appears to be continuous. A columnar phase is only observed for $L/D > 3$ at densities intermediate between the smectic and crystalline phases. The smectic-to-columnar transition is first order for $L/D \leq 5$. In the limit $L/D \rightarrow \infty$ this transition becomes continuous.

I. INTRODUCTION

Computer simulation is a powerful tool to investigate the thermodynamic properties and phase transitions of classical many-body systems. Simulations of well-defined microscopic model systems make it possible to establish the relation between thermodynamic behavior and interaction potential. A classical example is the molecular dynamics study by Alder and Wainwright[1] of the equation of state of hard spheres. These simulations showed that a liquid-solid transition can take place in a purely repulsive hard-core system. The precise location of the melting transition was subsequently determined by Hoover and Ree,[2] who computed the absolute free energy of both phases. Such simulations are interesting for three reasons. First of all, they demonstrate the possibility of crystallization of a concentrated hard-sphere fluid. But, in addition, they also provide "exact" numerical data to test approximate theoretical expressions for the equation of state[3] or statistical mechanical theories of the melting transition.[4] And finally, they allow us to gain a better understanding of the formation of real crystals, e.g., colloidal crystals in dispersions with short-range repulsive interparticle interactions.[5,6]

The hard-sphere model has turned out to be a useful reference system for simple (atomic) fluids and sterically stabilized[6] colloidal dispersions. It is, however, less well established to what extent hard-core models can help us to understand the phase behavior of systems where the interactions are no longer spherically symmetrical. In such systems, the ordering of translational and orientational degrees of freedom need not take place simultaneously. In principle, one or several partially ordered mesophases may form between the low-density isotropic fluid and the high-density solid. These liquid crystalline phases are characterized by long-range orientational order, possibly in combination with one- or two-dimensional translational order. In the absence of exact numerical results, the role of excluded volume effects in stabilizing the different liquid crystalline phases is still an open question.

At sufficiently high concentrations, colloidal solutions of rodlike[7,8] or platelike[9] particles undergo a first-order transition from the isotropic phase to a nematic liquid-crystalline phase. The latter is characterized by orientational order of the dispersed particles along a preferred direction. In 1949, Onsager[10] explained this phase transition as the result of the competition between the orientational entropy and the entropy effect associated with the orientation-dependent excluded volumes of hard anisometric particles. Recent computer simulations on infinitely thin hard platelets[11] and hard ellipsoids of revolution[12] confirm the importance of excluded volume effects in the formation of nematic phases in simple model systems.

In some colloidal dispersions[8] it has been observed experimentally that upon further increasing the density of the nematic phase, a smectic-A phase is generated by the onset of a one-dimensional density modulation along the direction of alignment. As the translational degrees of freedom perpendicular to the preferred direction are not affected, the structure within the layers remains liquid-like. Following the seminal work of McMillan,[13] the stability of such a layered structure is often attributed to the action of attractive forces. The loss of translational entropy involved in the layer formation is then compensated for by the associated gain in internal energy. More recently, Kloczkowski and Stecki[14] proposed a more detailed molecular model where hard-core repulsions, treated along the lines of the Onsager theory, as well as center-to-center attractions are taken into account. Their results illustrate, again, the essential role of hard

repulsions in stabilizing the nematic phase. However, these authors conclude that hard-core repulsions cannot explain the formation of the smectic phase. In fact, they state that "no smectic-A phase should ever be formed in systems of hard convex bodies." This statement seems to be supported by Dowell's[15] lattice model for systems of hard rods with two semiflexible tail chains. In the latter model, the stability of the smectic phase is due to the difference in steric packing between the rigid cores and the semiflexible tails. Inevitably, the smectic phase becomes intrinsically unstable in this model when these differences vanish by shortening the chains or by making them less flexible.

There is, however, experimental evidence that smectic ordering can occur in colloidal systems even under conditions where the colloidal particles have short-range repulsive interactions (e.g., β-FeOOH sols[16]). Theoretical evidence for the possible existence of hard-core smectic phases has been presented by Hosino *et al.*[17] However, the approximate nature of the theoretical description used in Ref. 17 does not rule out the possibility that the hard-core smectic phase predicted by Hosino *et al.* would disappear if a more rigorous approach were used.

Computer simulations on nonspherical hard-core model systems can help us to gain insight in the role of excluded volume effects in stabilizing a smectic phase and, more generally, any liquid-crystalline phase with partial translational order. As we want to focus on the density-induced freezing of the translational degrees of freedom, we eliminate the orientational degrees of freedom by artificially aligning the particles along the z axis. Parallel ellipsoids of revolution with eccentricity x, which are actually the simplest nonspherical hard-core particles, can be mapped onto hard spheres[18] by scaling all z coordinates with a factor $1/x$.

Consequently, we immediately turn to "second-choice" particles, i.e., spherocylinders consisting of a cylindrical segment of length L and diameter D capped at each end by a hemisphere of the same diameter. The shape is determined by the length-to-width ratio L/D. No scaling procedure exists which transforms a system of parallel spherocylinders to hard spheres, while leaving the partition function invariant. We therefore investigate the phase behavior for $L/D=0.25$, 0.50, 1, 2, 3, and 5 by Monte Carlo simulations. The computational techniques used to obtain the equation of state and the absolute free energy of all phases, are outlined in Sec. II. The different phase transitions which we observe in our model system are discussed in Sec. III. The phase behavior in the limit $L/D=0$ is established by the data of Hoover and Ree[2] on hard spheres. In Sec. III D we present data pertaining to hard parallel cylinders which provide information about the behavior in the limit $L/D\rightarrow\infty$. In Sec. III E we finally construct the phase diagram of hard parallel spherocylinders with L/D ratios between 0 and ∞.

II. COMPUTATIONAL TECHNIQUES

A. General aspects

In this section we give a survey of the numerical methods used to construct the phase diagram of the hard spherocylinder model system, i.e., the equation of state and absolute free energy of all fluid and crystalline phases. Most of the Monte Carlo simulations reported below were performed on systems of $N=90$ particles using periodic-boundary conditions. In some cases larger systems with up to $N=1080$ particles were simulated in order to check that the observed long-range correlations did not depend strongly on system size. We did not, however, carry out a systematic study of the system-size dependence of our results in all cases. All results presented below are expressed in the following reduced units: the density $\rho=Nv_0/V$ where v_0 is the molecular volume; the density $\rho^*=\rho/\rho_{cp}$ relative to the density of closest packing ρ_{cp}; the pressure $P^*=Pv_0/kT$; the chemical potential $\mu^*=\mu/kT$; the nth virial coefficient $B_n^*=B_n/B_2^{n-1}$ scaled with respect to the second virial coefficient B_2.

B. Monte Carlo method

In order to determine the equation of state of the fluid and crystalline phases, we performed simulations using the constant-pressure Monte Carlo (MC) method.[19,20] For our purpose, this method has obvious advantages over the constant-volume MC method. In the latter technique, knowledge of the value of the pair distribution function of hard-core particles at contact is required to compute the pressure. In the isothermal-isobaric N-P-T ensemble the volume (and hence the density) is obtained directly as an ensemble average. Moreover, a constant-P MC program is easily transformed into an isotropic-stress MC program[21] which allows us to study solid phases where both the shape and the volume of the crystal unit cell can change with pressure. As the Metropolis sampling scheme is now applied to each box edge independently rather than to the box volume, the crystal unit cell is allowed to relax to its equilibrium volume and shape. This is important for the free energy computation of the solid phase because any residual stress in the crystal may result in a significant increase in free energy.

The first step in the Monte Carlo simulations is the preparation of an acceptable initial configuration. Our systems were prepared by placing the spherocylinders with length-to-width ratio L/D on a regular close-packed lattice which was generated by distoring a face-centered-cubic lattice along its [111] axis by a factor $(1+L/D)$. This procedure implicitly assumes that the structure of a spherocylinder crystal is analogous to the regular close-packed structure of hard spheres. However, at lower densities this initial structure may, and in some cases does, transform to other (liquid-crystalline) structures. As the space-filling properties of the cylindrical and hemispherical parts of the spherocylinder are quite different, the density of closest packing turns out to be L/D dependent and ranges from $\rho_{cp}=0.7405$ for the case of hard spheres ($L/D=0$) to $\rho_{cp}=0.9069$ for hard cylinders ($L/D\rightarrow\infty$). An initial configuration for the generation of the fluid state points was obtained by expanding the close-packed structure to densities of approximately 25% of close packing, where it rapidly melted to form a translationally disordered nematic fluid.

Subsequent runs were always started from previously equilibrated configurations at higher (solid state points) or lower (fluid state points) pressure.

A cycle of a MC run in the N-PT ensemble consists of attempting to change the center-of-mass coordinates (x,y,z) of every particle once by adding random numbers $(\Delta x,\Delta y,\Delta z)$, followed by an attempt to change the box volume V with a randomly chosen amount ΔV. The magnitudes of these trial moves were such that typically 30% of the particle displacements and volume changes were accepted. A typical run consisted of 10^4 to 2×10^4 such cycles, excluding equilibration. The relative error in the volume (or equivalently density) is of the order of 1%. Some runs, especially in the vicinity of a phase transition, were much longer. Nevertheless, the large pretransitional fluctuations resulted in a loss of accuracy (relative errors of 3–5 %).

We also computed the first five virial coefficients of the fluid branch, which allows us to test the low-density MC results. In fact, only the virial coefficients 3–5 had to be evaluated by Monte Carlo, using the diagram technique developed by Ree and Hoover.[22] As in the case of hard spheres, the second virial coefficient equals four times the molecular volume.

C. Free-energy computations

Knowledge of the equation of state of the fluid and solid phase does not suffice to locate a first-order fluid-solid phase transition. The reason is that, in a finite periodic system, the fluid can be overcompressed and the solid overexpanded appreciably. As a consequence the densities of the coexisting phases cannot be determined directly. To locate the fluid-solid tie line, the absolute Helmholtz free energy of both phases must be computed.

The free-energy computation of a fluid phase at any density ρ poses no particular problem. The free energy per particle (expressed in units kT) is simply the sum of an ideal and an excess contribution. The latter corresponds to the difference between the free energy of the fluid at density ρ and that of an ideal gas at the same density,

$$\frac{F(\rho)}{NkT}=\frac{F_{\text{ideal gas}}(\rho)}{NkT}+\int_0^{\rho}[P^*(\rho')-P^*_{\text{ideal gas}}(\rho')]\frac{d\rho'}{\rho'^2}\ , \tag{1}$$

where $P^*(\rho')$ can be obtained by computer simulations. To carry out the integration in Eq. (1), the $P^*(\rho')$ data are first fitted to a convenient analytical form. We used the generalized y expansion to fit our MC data,

$$P^*(\rho')=\sum_{n=1}^{m}C_n^*y^n\ ,$$

where $y=\rho'/(1-\rho')$. Originally the y expansion[23] was proposed by Barboy and Gelbart. These authors observed that for a number of hard-core fluids, the y expansion converges more rapidly to the true equation of state than the corresponding virial series. The expansion coefficient C_n^* is related to the n first virial coefficients $B_1^*, B_2^*, \ldots, B_n^*$,

$$C_n^*=\sum_{k=0}^{n-1}\binom{n-1}{k}(-1)^{n-k-1}4^kB_{k+1}^*\ . \tag{2}$$

In our case however, we use the y expansion simply as an efficient way to parametrize the MC data. The number of terms (m) was fixed by the requirement that increasing m did not significantly lower the χ^2 of the fit.

The absolute free energy of the solid phase is computed by using the Einstein crystal method described in Ref. 24. This method is similar in spirit to the one used to obtain the free energy of a fluid by constructing a reversible path to the ideal-gas reference state, the free energy of which is known. Similarly, we can construct a reversible path from an arbitrary crystalline solid to an Einstein crystal with the same structure. The Hamiltonian of an N-particle Einstein crystal is

$$H(\lambda_{\max})=H_0+\lambda_{\max}\sum_{i=1}^{N}(\mathbf{r}_i-\mathbf{r}_i^0)^2\ , \tag{3}$$

where H_0 is the Hamiltonian of the unconstrained hard-core solid and $(\mathbf{r}_i-\mathbf{r}_i^0)$ the displacement of particle i from its lattice site. $\lambda_{\max}$ is the harmonic spring constant of the Einstein crystal. For sufficiently large values of $\lambda_{\max}$, the partition function $Q_N^{\text{Einst}}(\lambda_{\max})$ is approximately equal to the partition function of a perfect Einstein crystal. This approximation becomes rigorously exact in the limit $\lambda_{\max}\to\infty$ where all particle interactions are prevented by the infinitely strong constraints,

$$Q_N^{\text{Einst}}(\lambda_{\max})=N^{-3/2}\left[\frac{\pi kT}{\lambda_{\max}}\right]^{3(N-1)/2}\ . \tag{4}$$

The free energy of our unconstrained hard spherocylinder solid with $\lambda=0$ reads

$$\frac{F_N(\lambda=0)}{NkT}=\frac{F_N^{\text{Einst}}(\lambda_{\max})}{NkT}-\frac{\Delta F_{MC}}{NkT}-\frac{\ln V}{N}\ . \tag{5}$$

The third term in Eq. (5) takes into account that both F_N^{Einst} and ΔF_{MC} are computed in a fixed center-of-mass system[24] where the free energy per particle is $(\ln V/N)$ higher than in an unconstrained system. ΔF_{MC} is the difference in free energy per particle between the interacting Einstein crystal with $\lambda=\lambda_{\max}$ and the solid under consideration,

$$\begin{aligned}\Delta F_{\text{MC}}&=\int_0^{\lambda_{\max}}\left[\frac{\partial F}{\partial\lambda}\right]_{\lambda}d\lambda\\&=\int_0^{\lambda_{\max}}\left\langle\sum_{i=1}^{N}(\mathbf{r}_i-\mathbf{r}_i^0)^2\right\rangle_{\lambda}d\lambda\ .\end{aligned} \tag{6}$$

In order to obtain the mean-square particle displacements as functions of the spring constant λ, we have to carry out additional MC simulations. The integral in (6) was evaluated by 10-point Gauss-Legendre quadrature. At each integration point, we performed a MC run of 10^4 trial moves per particle to obtain the mean-square particle displacements with sufficient accuracy.

Combining the data on the equation of state and the absolute free energy, we can locate the points where the pressure P and the chemical potential $\mu=(F+PV)/N$ of

two phases are simultaneously equal. The densities of the phases in thermodynamic equilibrium are determined by solving the coexistence equations using an iterative numerical method.

III. RESULTS

A. General aspects

Figure 1 shows the equation-of-state data for hard parallel spherocylinders with length-to-width ratios $L/D=0.25$, 0.50, 1, 2, 3, and 5 as obtained by constant-pressure or isotropic-stress Monte Carlo simulations on systems of $N=90$ particles. The data points have been collected in Tables I and II. The five-term virial equations of state, which are also displayed in Fig. 1, allow us to check the low-density behavior of the fluid branch. The virial coefficients are collected in Table III. The parameters describing the fits through the MC data are shown in Table IV, whereas the results of the free-

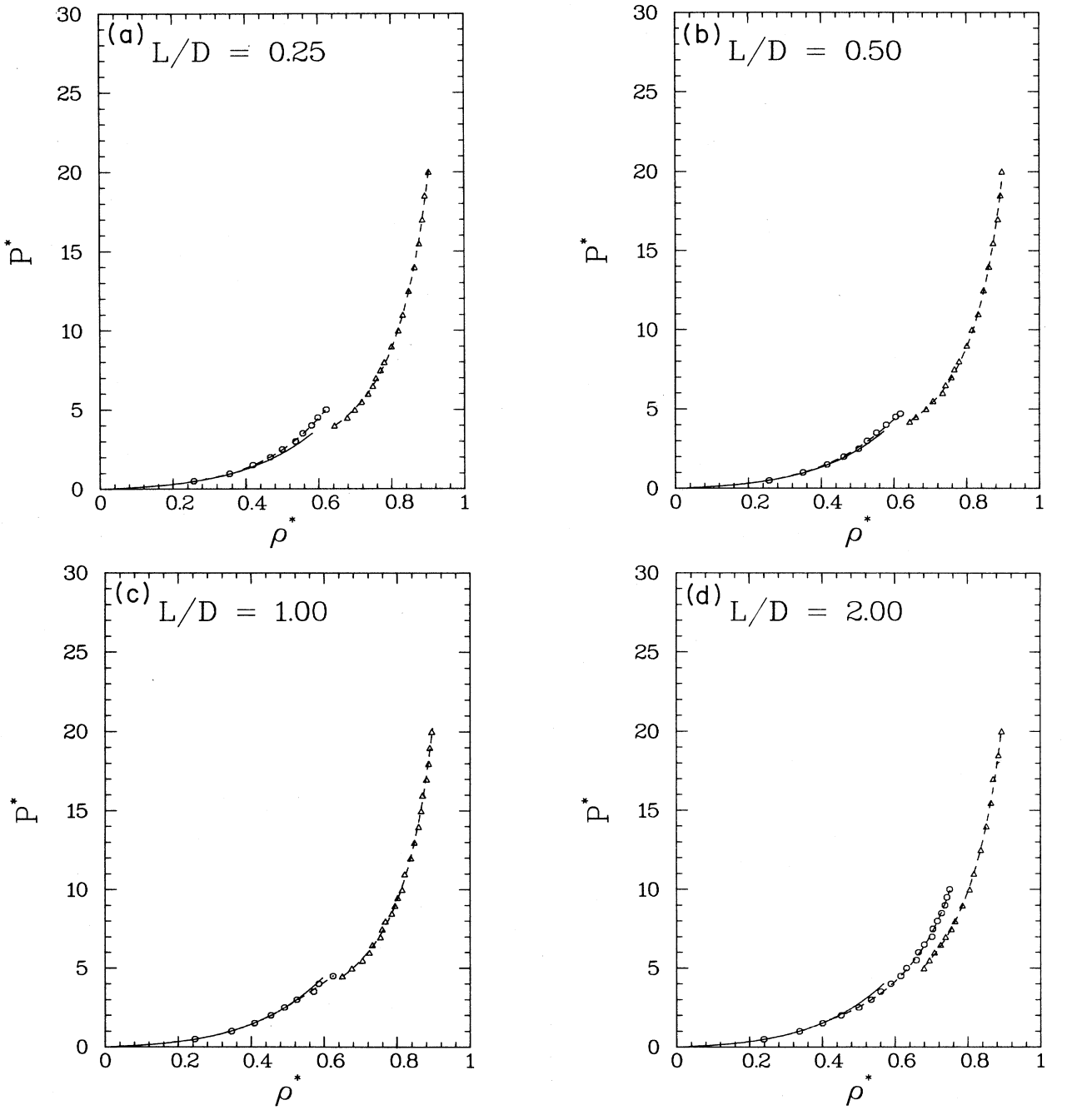

FIG. 1. Equation-of-state data of hard parallel spherocylinders with length-to-width ratios $L/D=$(a) 0.25, (b) 0.5, (c) 1, (d) 2, (e) 3, and (f) 5. The reduced density $\rho^*=\rho/\rho_{cp}$ where ρ_{cp} is the density of closest packing and the pressure $P^*=Pv_0/kT$ where v_0 is the molecular volume. Open circles, low-density fluid branch; open triangles, solid branch; plusses, columnar branch ($L/D=5$); solid lines, five-term virial series; dashed lines, fits through the MC data.

energy computations are compiled in Table V.

In order to monitor the local structure of the hard spherocylinder fluid and, more specifically, to detect the possible onset of translational order, we computed different components of the orientationally averaged pair distribution function $g_2(r)$. In particular, we collected the longitudinal correlation function $g_{\parallel}(z)$ and the transverse correlation function $g_{\perp}(r_{\perp})$. The reason to monitor $g_{\parallel}(z)$ and $g_{\perp}(r_{\perp})$ separately is that they are sensitive probes of translational ordering respectively parallel and perpendicular to the direction of molecular alignment (the z axis). In contrast, the usual pair distribution function $g_2(r)$ is sensitive to three-dimensional crystalline ordering. Unlike $g_2(r)$, $g_{\parallel}(z)$, and $g_{\perp}(r_{\perp})$ need not go to zero as the argument approaches zero because these functions describe correlations in the particle positions projected along the z axis and in the xy plane, respectively.

A first inspection of Fig. 1 reveals a strong L/D dependence of the general behavior of the equations of state. We notice, for instance, in the $L/D=5$ system, the existence of an additional third branch intermediate to the low-density fluid and the high-density solid. The corresponding phase is discussed in Sec. III B. For spherocylinders with $L/D>0.5$, the five-term virial expansion accurately represents the low-density fluid state points, but at higher densities it tends to overestimate the pressure. This is quite unexpected because for $L/D\leq 0.5$ we find the normal hard-sphere behavior, namely, that neglecting the sixth and higher contributions in the virial series results in an underestimation of the pressure. On the basis of the equation-of-state data alone it is impossible to tell what causes this unusual behavior. However, in Sec. III C we show that structural data suggest that for $L/D\geq 0.5$, a second-order phase transition to the smectic phase takes place in the same density range where the Monte Carlo pressure starts to fall below the five-term virial series prediction.

Finally, for $L/D=0.25$, 0.50, and 1, we observe spontaneous crystallization of the hard-spherocylinder fluid. Such spontaneous freezing upon compression is, in fact, rather unusual for hard-core fluids. The system composed of spherocylinders with $L/D=1$ exhibits almost no hysteresis at the fluid-solid transition. This suggests that, for this particular system, the limits of thermodynamical and mechanical stability of the fluid and solid phases nearly coincide. We can reversibly transform the fluid to the solid, and vice versa, by changing the pressure by 0.1 in reduced units. Consequently, for this particular case, the limit of mechanical stability of the fluid and solid phase provide an accurate estimate of the thermodynamic melting point.

B. The columnar phase

Spherocylinders with $L/D>3$ exhibit a more complicated phase behavior. For these systems, a third branch, intermediate between the low-density fluid and high-density solid, is observed (Fig. 1). As we shall show below, this branch corresponds to a columnar liquid crystalline phase characterized by two-dimensional long-range translational order. This additional phase is obtained by expanding the initial fcc lattice, until it melts at a density of approximately 80% of close packing. Subsequently, the newly formed phase can be compressed appreciably without recrystallizing. Such hysteresis is typical of a first-order phase transition. The difference in structural properties of both phases can

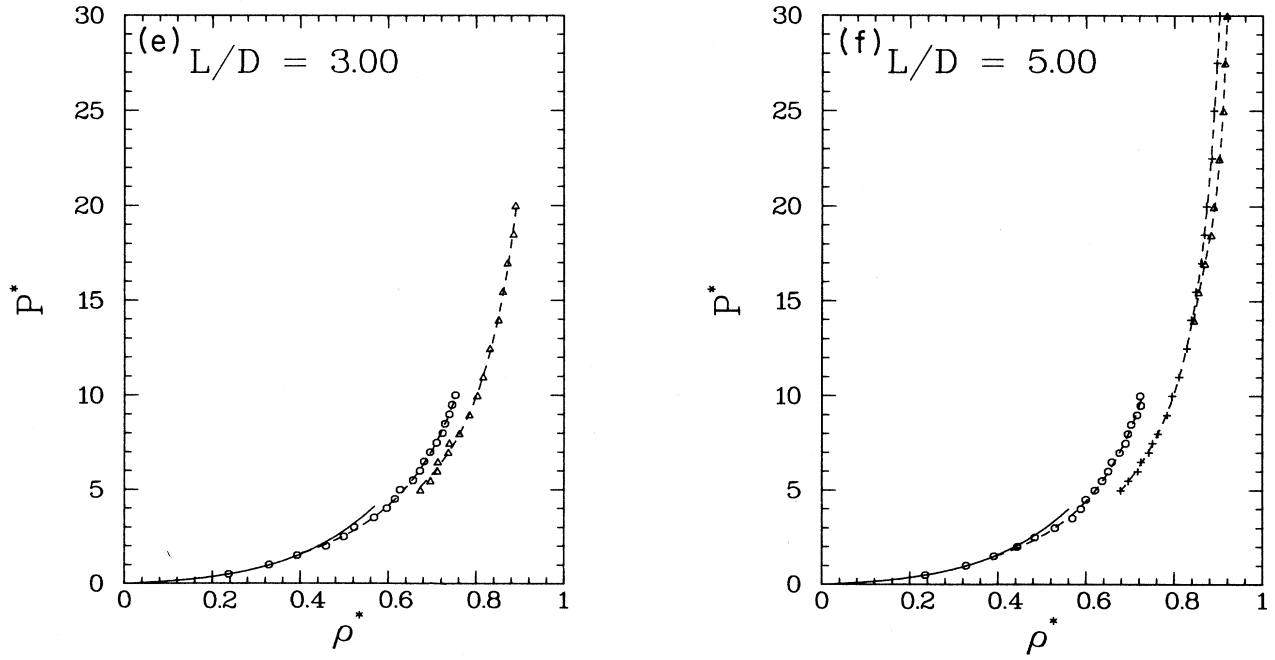

FIG. 1. (*Continued*).

TABLE I. Equation-of-state data for the fluid phases of hard parallel spherocylinders with length-to-width ratios $L/D=0.25$, 0.5, 1, 2, 3, and 5. For the case $L/D=5$, column (a) gives the data for the low-density (nematic + smectic) branch and column (b) the data for the columnar branch. The density $\rho^*=\rho/\rho_{cp}$ where ρ_{cp} is the density of closest packing and the pressure $P^*=Pv_0/kT$ where v_0 is the molecular volume.

$L/D=0.25$		$L/D=0.50$		$L/D=1.00$		$L/D=2.00$		$L/D=3.00$		(a) $L/D=5.00$		(b) $L/D=5.00$	
P^*	ρ^*	P^*	ρ^*	P^*	ρ^*	P^*	ρ^*	P^*	ρ^*	P^*	ρ^*	P^*	ρ^*
0.5	0.257	0.5	0.257	0.5	0.246	0.5	0.239	0.5	0.237	0.5	0.235	5.0	0.678
1.0	0.356	1.0	0.350	1.0	0.346	1.0	0.337	1.0	0.329	1.0	0.327	5.5	0.696
1.5	0.419	1.5	0.416	1.5	0.409	1.5	0.401	1.5	0.393	1.5	0.391	6.0	0.717
2.0	0.467	2.0	0.462	2.0	0.454	2.0	0.452	2.0	0.459	2.0	0.444	6.5	0.724
2.5	0.500	2.5	0.503	2.5	0.491	2.5	0.500	2.5	0.499	2.5	0.484	7.0	0.742
3.0	0.536	3.0	0.526	3.0	0.525	3.0	0.534	3.0	0.522	3.0	0.530	7.5	0.751
3.5	0.556	3.5	0.552	3.5	0.571	3.5	0.560	3.5	0.567	3.5	0.569	8.0	0.763
4.0	0.581	4.0	0.578	4.0	0.586	4.0	0.588	4.0	0.597	4.0	0.588	9.0	0.783
4.5	0.598	4.1	0.590	4.5	0.624	4.5	0.615	4.5	0.615	4.5	0.599	10.0	0.795
5.0	0.621	4.2	0.601			5.0	0.631	5.0	0.627	5.0	0.620	11.0	0.811
		4.3	0.615			5.5	0.658	5.5	0.656	5.5	0.637	12.5	0.828
		4.4	0.602			6.0	0.664	6.0	0.672	6.0	0.650	14.0	0.838
		4.5	0.604			6.5	0.680	6.5	0.681	6.5	0.658	15.5	0.849
		4.6	0.613			7.0	0.701	7.0	0.695	7.0	0.676	17.0	0.861
		4.7	0.618			7.5	0.704	7.5	0.710	7.5	0.690	18.5	0.868
						8.0	0.716	8.0	0.723	8.0	0.695	20.0	0.872
						8.5	0.728	8.5	0.729	8.5	0.703	22.5	0.884
						9.0	0.737	9.0	0.739	9.0	0.716	25.0	0.889
						9.5	0.742	9.5	0.745	9.5	0.724	27.5	0.897
						10.0	0.750	10.0	0.752	10.0	0.723	30.0	0.902

TABLE II. Equation-of-state data for the solid phase of hard parallel spherocylinders with length-to-width ratios $L/D=0.25$, 0.5, 1, 2, 3, and 5. Reduced units as in Table I.

$L/D=0.25$		$L/D=0.50$		$L/D=1.00$		$L/D=2.00$		$L/D=3.00$		$L/D=5.00$	
P^*	ρ^*	P^*	ρ^*	P^*	ρ^*	P^*	ρ^*	P^*	ρ^*	P^*	ρ^*
4.0	0.644	4.2	0.643	4.5	0.650	5.0	0.679	5.0	0.673	14.0	0.844
4.5	0.679	4.3	0.650	5.0	0.676	5.5	0.694	5.5	0.696	15.5	0.855
5.0	0.699	4.4	0.654	5.5	0.705	6.0	0.708	6.0	0.712	17.0	0.869
5.5	0.718	4.5	0.660	6.0	0.723	6.5	0.725	6.5	0.713	18.5	0.883
6.0	0.735	5.0	0.688	6.5	0.732	7.0	0.739	7.0	0.737	20.0	0.889
6.5	0.748	5.5	0.707	7.0	0.754	7.5	0.755	7.5	0.739	22.5	0.901
7.0	0.757	6.0	0.734	7.5	0.759	8.0	0.764	8.0	0.762	25.0	0.910
7.5	0.770	6.5	0.742	8.0	0.767	9.0	0.785	9.0	0.784	27.5	0.914
8.0	0.780	7.0	0.758	8.5	0.785	10.0	0.805	10.0	0.802	30.0	0.919
9.0	0.790	7.5	0.766	9.0	0.794	11.0	0.817	11.0	0.816		
10.0	0.819	8.0	0.779	9.5	0.802	12.5	0.836	12.5	0.831		
11.0	0.831	9.0	0.800	10.0	0.814	14.0	0.851	14.0	0.851		
12.5	0.847	10.0	0.815	11.0	0.820	15.5	0.864	15.5	0.860		
14.0	0.863	11.0	0.832	12.0	0.837	17.0	0.870	17.0	0.871		
15.5	0.876	12.5	0.846	13.0	0.847	18.5	0.885	18.5	0.885		
17.0	0.885	14.0	0.861	14.0	0.858	20.0	0.894	20.0	0.889		
18.5	0.892	15.5	0.873	15.0	0.865						
20.0	0.903	17.0	0.886	16.0	0.870						
		18.5	0.893	17.0	0.880						
		20.0	0.898	18.0	0.886						
				19.0	0.889						
				20.0	0.895						

TABLE III. Virial coefficients of hard parallel spherocylinders with length-to-width ratios $L/D=0.25$, 0.5, 1, 2, 3, and 5 as well as $L/D=0$ (hard spheres) and $L/D\to\infty$ (hard parallel cylinders). The virial coefficient $B_n^*=B_n/B_2^{n-1}$ is scaled with respect to the second virial coefficient B_2, which equals four times the molecular volume. In the case of the hard-sphere fluid, the third and fourth virial coefficient are known exactly ($B_3^*=0.6250$; $B_4^*=0.2869$) and the most accurately known (Ref. 2) value of $B_5^*=0.1100\pm0.0003$.

L/D	B_3^*	B_4^*	B_5^*
0	0.6249±0.0004	0.2876±0.0006	0.1100±0.0008
0.25	0.6235±0.0004	0.2846±0.0006	0.1072±0.0008
0.50	0.6204±0.0004	0.2782±0.0007	0.1008±0.0009
1.00	0.6140±0.0004	0.2671±0.0006	0.0908±0.0008
2.00	0.6059±0.0004	0.2517±0.0007	0.0750±0.0009
3.00	0.6012±0.0004	0.2444±0.0007	0.0686±0.0009
5.00	0.5968±0.0004	0.2362±0.0006	0.0618±0.0010
$L/D\to\infty$	0.5858±0.0004	0.2179±0.0007	0.0479±0.0010

best be visualized by displaying $g_{\parallel}(z)$ and $g_{\perp}(r_{\perp})$ (Fig. 2). The absence of translational order in the z direction in the columnar phase results in a liquidlike $g_{\parallel}(z)$ correlation function whereas the solidlike behavior of $g_{\perp}(r_{\perp})$ reflects the two-dimensional crystalline order in the xy plane perpendicular to the columns. Snapshots of typical molecular configurations clearly show order in the xy plane and disorder along the z axis in the case of the columnar phase (Fig. 3). Similar striking differences between $g_{\parallel}(z)$ and $g_{\perp}(r_{\perp})$ were observed for all state points on the two high-density branches for $L/D=5$ in Fig. 1. Although we have not performed a systematic analysis of the statistical errors in the radial distribution functions, the fact that different simulations of the same state point always yielded indistinguishable distribution functions suggests that these errors are less than or equal to 5%. It should be noted that Fig. 2 was computed for $N=270$ spherocylinders. We found the same behavior for $N=90$. We stress, however, that the absence of a noticeable system-size dependence for $90\leq N\leq 270$, al-

TABLE IV. Coefficients for the y-expansion fits to the Monte Carlo equation-of-state data: $P^*=\Sigma_n C_n^* y^n$ where $y=\rho/(1-\rho)$. The range of validity of the different fits is given in column 3. We refer to Table III for the coefficients of the five-term virial expansion, which accurately represents the low-density fluid state points. For $L/D=0.25$ and 0.5, the exact C_1^* and C_2^* are used, which are related to the virial coefficients by $C_1^*=B_1^*$ and $C_2^*=4B_2^*-B_1^*$.

L/D	Phase	Pressure interval	Expansion type	C_1^*	C_2^*	C_3^*	C_4^*	C_5^*
0.25	fluid	0.0–5.0	Y	1	3	3.596	−1.932	
	solid	4.0–20.0	Y	4.331	−1.927	1.539		
0.50	fluid	0.0–4.7	Y	1	3	3.684	−2.882	
	solid	4.2–20.0	Y	4.893	−2.223	1.253		
1.00	fluid	0.0–2.5	B					
	fluid	2.5–4.5	Y	0.302	6.971	−3.139		
	solid	4.5–20.0	Y	4.125	−1.089	0.690		
2.00	fluid	0.0–1.5	B					
	fluid	1.5–10.0	Y	2.313	1.175	0.318		
	solid	5.0–20.0	Y	2.814	0.309	0.210		
3.00	fluid	0.0–1.5	B					
	fluid	1.5–10.0	Y	2.376	1.020	0.244		
	solid	5.0–20.0	Y	3.254	−0.028	0.216		
5.00	fluid	0.0–1.5	B					
	fluid	1.5–10.0	Y	2.141	1.065	0.460		
	column	5.0–30.0	Y	0.402	3.454	−1.358	0.242	
	solid	14.0–30.0	Y	−64.061	60.059	−17.508	1.716	
$L/D\to\infty$	fluid	0.0–1.5	B					
	fluid	1.5–3.5	Y	1.713	2.245	−0.623		
	column	3.5–20.0	Y	9.059	−10.190	5.857	−1.373	0.118

TABLE V. Contributions to the free energy of a solid phase (a) or a columnar phase (b) of hard parallel spherocylinders with length-to-width ratios $L/D=0.25$, 0.5, 1, 2, 3, and 5 and $L/D\rightarrow\infty$. The computations were performed on systems of $N=90$ particles. All contributions are expressed per particle and in units kT. (a) $F_N(\lambda_{\max})=F_N^{\text{Einst}}(\lambda_{\max})-\ln V/N$: free energy of a noninteracting three-dimensional Einstein crystal with spring constant $\lambda_{\max}$. ΔF_{MC}: Monte Carlo result for the free-energy difference between an interacting Einstein crystal ($\lambda=\lambda_{\max}$) and the unconstrained solid ($\lambda=0$) at the same density ρ^*. The spring constant $\lambda_{\max}$ is chosen sufficiently large to guarantee that the free-energy difference between the interacting and noninteracting Einstein crystal is negligible. $F_N(\rho^*)$: absolute free energy per particle of the N-particle solid at density ρ^* [Eq. (5)]. (b) $F_N(\lambda_{\max})=F_N^{\text{Einst}}(\lambda_{\max})+F_M^z-\ln A/N$: contribution of the two-dimensional noninteracting Einstein crystal and of the columnar fluids to the total free energy $F_N(\rho^*)$ of a columnar phase [Eq. (8)].

L/D	ρ^*	$\lambda_{\max}$	$F_N(\lambda_{\max})$	ΔF_{MC}	$F_N(\rho^*)$
			(a)		
0.25	0.770	2000	9.600	4.32±0.02	5.278
0.50	0.766	2000	0.597	4.61±0.02	4.991
1.00	0.759	2000	9.594	5.02±0.02	4.571
2.00	0.755	2000	9.589	5.52±0.03	4.066
3.00	0.739	2000	9.585	6.08±0.03	3.507
5.00	0.855	6000	11.212	6.03±0.03	5.185
			(b)		
5.00	0.751	1000	5.160	2.16±0.01	2.998
$L/D\rightarrow\infty$	0.768	1000	5.771	2.04±0.01	3.733

though suggestive, should not be interpreted as solid evidence for the absence of any dependence of the relative stability of the crystalline and liquid crystalline phases on the size of the system.

In order to locate the first-order phase transition from columnar to crystalline phase, we use a modification of the Einstein crystal method described above to compute the free energy of the columnar phase. In this case, we use as a reference state a system where the particles are ordered in the xy plane by harmonic springs $\lambda_{\max}$ (two-dimensional Einstein crystal), while they are free to slide along the column axes. In the limit $\lambda_{\max}\rightarrow\infty$, the columnar fluids become effectively one dimensional because the constraints in the xy plane confine the centers of mass of the particles to the axes of parallel columns. The free energy of the latter system was evaluated analytically by Tonks[25] in 1936. Taking into account the effect of periodic-boundary conditions, the expression for the partition function of a M-particle one-dimensional hard-rod fluid becomes

$$Q_M^z=\frac{1}{M!}L_z(L_z-ML')^{(M-1)}\ , \tag{7}$$

where L_z is the length of the box edge along the z axis. In the limit $\lambda_{\max}\rightarrow\infty$, the effective length L' of the rods is given by $L'=L+D$.

Similar to Eq. (5) we write F_N per particle and in units kT, as follows:

$$\frac{F_N}{NkT}=\frac{F_N^{\text{Einst}}(\lambda_{\max})}{NkT}+\frac{F_M^z}{MkT}-\frac{\Delta F_{\text{MC}}}{NkT}-\frac{\ln A}{N}\ , \tag{8}$$

where $(\ln A/N)$ corrects for the use of a fixed center of mass in the xy plane and F_M^z is the contribution to the total free energy of the M-particle columnar fluids. The spring constant $\lambda_{\max}$ is chosen sufficiently large to guarantee that corrections to the partition function Q_N^{Einst} of the perfect two-dimensional Einstein crystal due to lateral hard-core overlaps are negligible,

$$Q_N^{\text{Einst}}(\lambda_{\max})=N^{-1}\left[\frac{\pi kT}{\lambda_{\max}}\right]^{N-1}\ . \tag{9}$$

The free-energy difference ΔF_{MC} between the interacting Einstein crystal ($\lambda=\lambda_{\max}$) and the unconstrained two-dimensional solid ($\lambda=0$) is computed by MC simulations [Eq. (6)].

The results of the free-energy computation of the columnar phase for $L/D=5$ are shown in Table 5(b).

C. The nematic-smectic phase transition

As mentioned above, Fig. 1 shows that for spherocylinders with $L/D>0.5$, a five-term virial approximation to the equation of state tends to overestimate the pressure of the dense fluid. Closer inspection reveals that, dependent on the L/D ratio, the equations of state actually change slope at densities between 40% and 60% of close packing. We did not observe a similar behavior in a fluid of spherocylinders with $L/D=0.25$. For the latter system the pressure increases monotonically with density. The presence of a change of slope for $L/D\geq 0.50$ suggests the possible occurrence of an (almost) second-order phase transition.

In order to gain some insight into the possible nature of such a phase transition, we studied the behavior of $g_{\parallel}(z)$ and $g_{\perp}(r_{\perp})$ at densities both below and above the cusp in the equation of state. An example of the behavior of $g_{\parallel}(z)$ and $g_{\perp}(r_{\perp})$ is shown in Fig. 4. The correlation functions correspond to a system of $N=270$ sphero-

cylinders with $L/D=5$, at densities $\rho^*=0.24$ ($P^*=0.5$) and $\rho^*=0.62$ ($P^*=5.0$), respectively. Unlike $g_\perp(r_\perp)$, which obviously remains liquidlike, $g_\parallel(z)$ is seen to develop strong periodic oscillations characteristic for a layered structure. The absence of translational order within the layers indicates that we are actually dealing with a smectic-A phase. This is further corroborated by snapshots of molecular configurations in Fig. 5. We refer to Fig. 3 for comparison with a three-dimensional crystalline structure. This structural information leaves open the possibility that the observed layered phase is actually a hexatic B rather than a smectic-A phase. We,

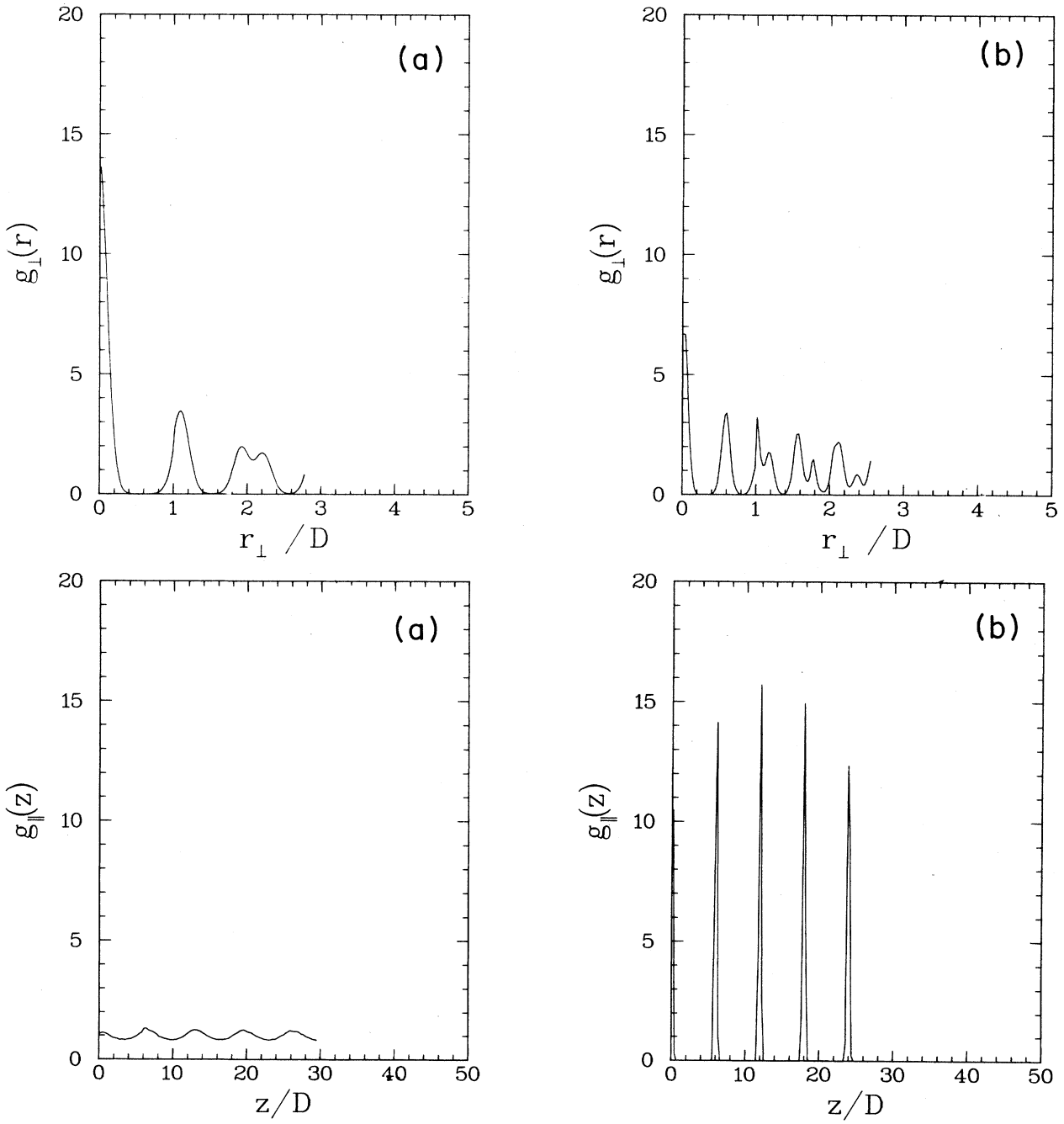

FIG. 2. Transverse correlation function $g_\perp(r_\perp)$ and longitudinal correlation function $g_\parallel(z)$ corresponding to a system of 270 parallel spherocylinders with $L/D=5$, at densities $\rho^*=0.75$ [columnar phase (a)] and $\rho^*=0.91$ [solid phase (b)]. The liquidlike behavior of $g_\parallel(z)$ in the columnar phase reflects the absence of translational order in the direction of the particle axes. Snapshots of molecular configurations of the system at the same densities are shown in Fig. 3.

however, also observed that the bond-orientational correlation function decayed within one molecular diameter.

We found no hysteresis effects upon slowly compressing and subsequently expanding the system in the vicinity of the point $\rho^* = 0.56$ where the one-dimensional density modulation sets in. This suggests that the nematic phase is transformed into the smectic phase through a continuous phase transition. At the transition we observed the characteristic divergence of the peaks in the longitudinal structure factor $S(k_z)$, corresponding to smectic fluctuations in the nematic fluid. This effect is

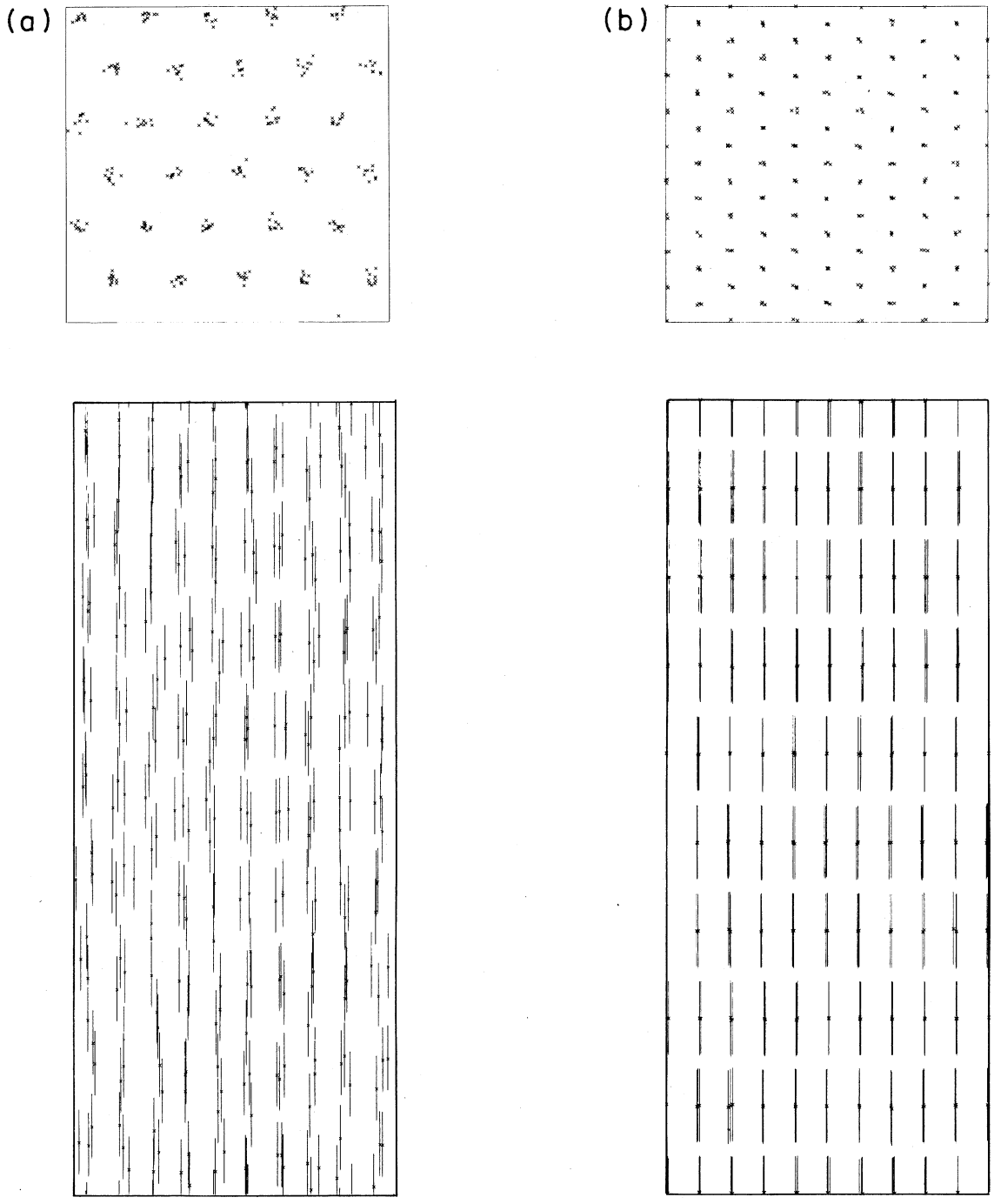

FIG. 3. Snapshots of typical molecular configurations of a system of 270 spherocylinders with $L/D = 5$. (a) Columnar phase ($\rho^* = 0.75$). (b) Solid phase ($\rho^* = 0.91$). The upper figures show a projection in the plane perpendicular to the molecular axes; the lower figures show a projection in a plane parallel to the direction of alignment. The spherocylinders are indicated by a line segment of length L.

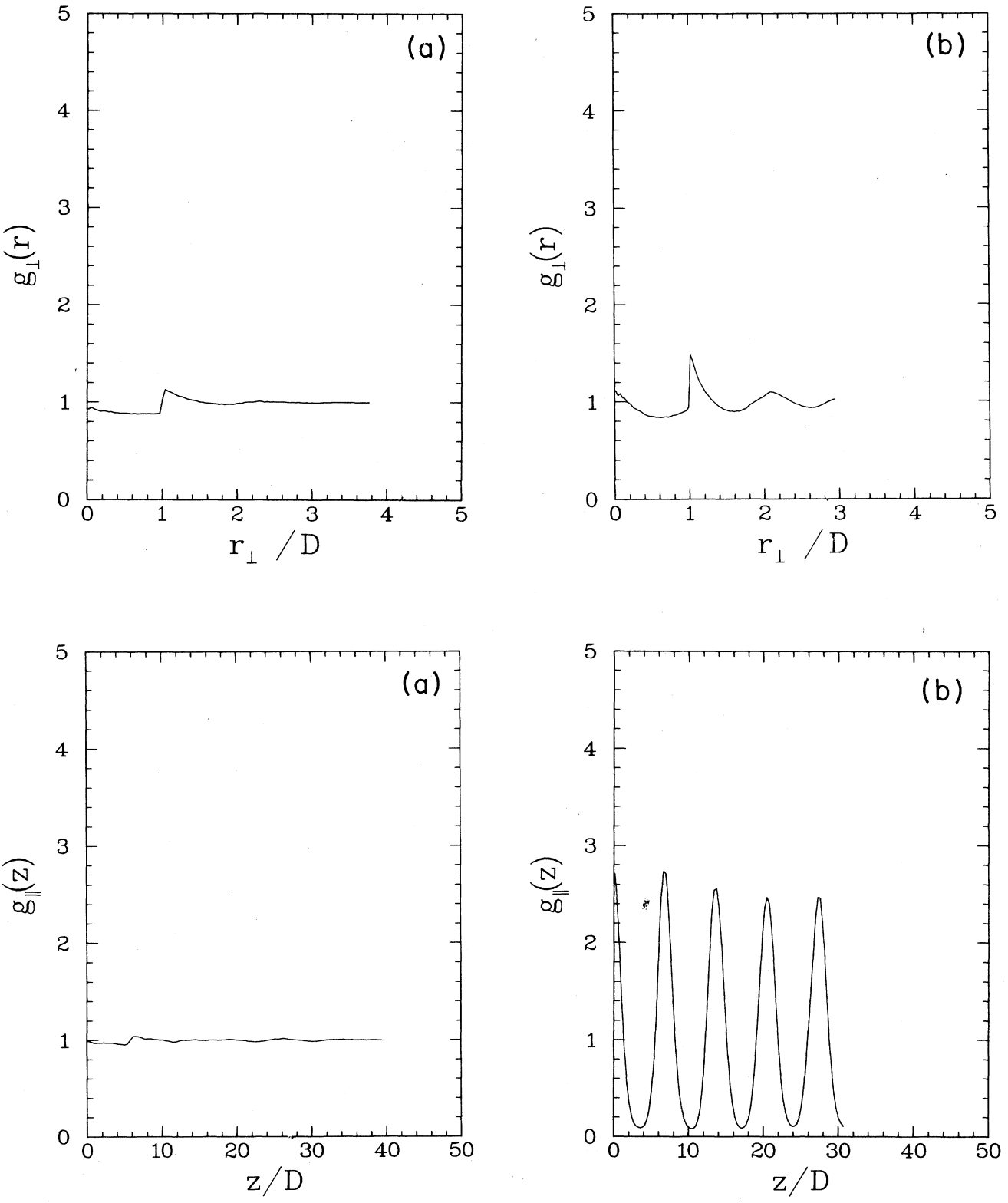

FIG. 4. Transverse correlation function $g_\perp(r_\perp)$ and longitudinal correlation function of $g_\parallel(z)$ corresponding to a system of 270 parallel spherocylinders with $L/D=5$, at densities $\rho^*=0.24$ [nematic phase (a)] and $\rho^*=0.62$ [smectic phase (b)]. The periodic oscillations of $g_\parallel(z)$ in the smectic phase are caused by a one-dimensional density modulation along the direction of alignment. The liquidlike $g_\perp(r_\perp)$ reflects the absence of translational order within the layers. Snapshots of molecular configurations of the system at the same densities are shown in Fig. 5.

shown in Fig. 6 where the inverse value of $S(k_{max})$ is displayed as a function of the density. The wave vector $k_z = k_{max}$ corresponds to the first maximum in $S(k_z)$. The position of the first maximum allows us to calculate the periodicity d of the layered structure by $d = 2\pi/k_{max}$ and hence the number of layers that fits into the box (Fig. 7). It appears that as the system is compressed, the number of layers varies from 11 at low densities to nine at high densities (the latter number corresponds to the number of crystalline layers that fits into the periodic box), whereas the interlayer spacing remains approximately constant. This observation indicates that we are

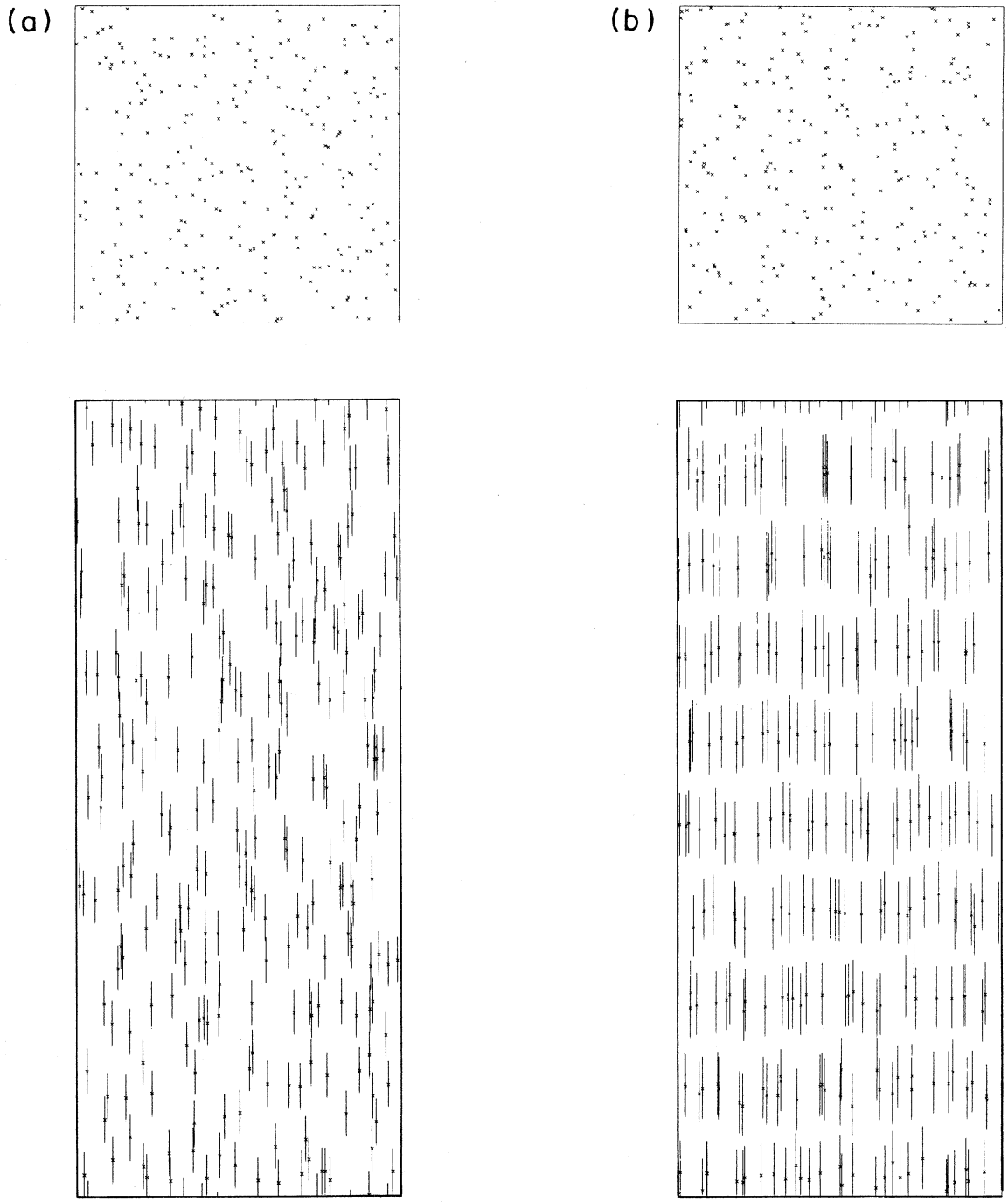

FIG. 5. Snapshots of typical molecular configurations of a system of 270 spherocylinders with $L/D = 5$. (a) Nematic phase ($\rho^* = 0.24$). (b) Smectic phase ($\rho^* = 0.62$). The upper figures show a projection in the plane perpendicular to the molecular axes; the lower figures show a projection in a plane parallel to the direction of alignment. The spherocylinders are indicated by a line segment of length L.

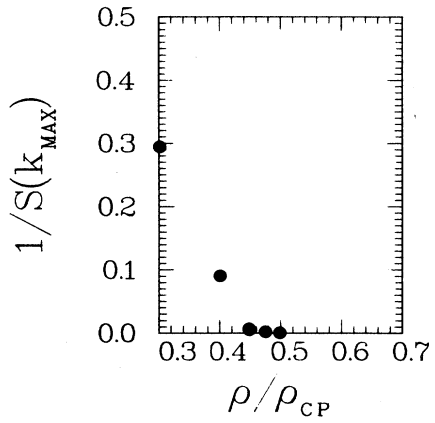

FIG. 6. Density dependence of the first maximum in the longitudinal structure factor of parallel spherocylinders with $L/D=5$. The ordinate shows $1/S(k_{\max})$. In the dilute fluid, this quantity approaches one. In a smectic phase it should vanish in the thermodynamic limit. The present results apply to a 270-particle system, hence $1/S(k_{\max}) \geq 1/270$.

not dealing with residual crystalline order caused by incomplete melting because in the latter case the number of layers at low densities would also be equal to nine. The density modulation is not affected by increasing the system size from 90 to 1080 particles. Actually, the peaks are even somewhat sharper in the larger systems. This suggests that the observed effect is not an artifact induced by the periodic-boundary conditions.

Applying a similar analysis to the systems with smaller L/D ratios, indicates that a continuous nematic-smectic phase transition occurs for all spherocylinders with $L/D \geq 0.5$. The change of slope of the equation of state for $L/D=0.50$ is not visible because the nematic-to-smectic transition is very close to the limit of mechanical stability of the fluid. The transition densities, as well as the corresponding pressure and chemical potential, are collected in Table VII(a).

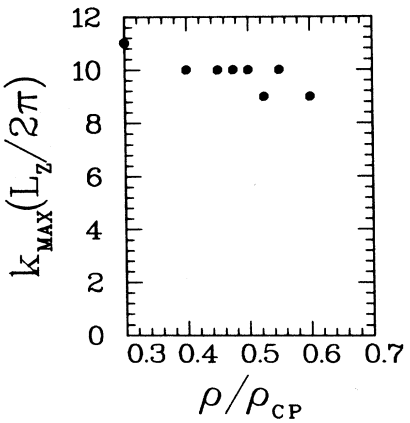

FIG. 7. Density dependence of the number of layers in a system of 270 parallel spherocylinders with $L/D=5$. The number of layers is defined as the number of oscillations of the largest longitudinal Fourier component in the periodic box, $k_{\max}L_z/2\pi$. Note that the number of layers changes on compression.

D. Phase behavior of hard parallel spherocylinders in the limit $L/D \to \infty$

Hard parallel spherocylinders exhibit a strongly L/D-dependent phase behavior which has to be attributed completely to the difference in packing properties between the cylindrical segment and the hemispherical caps. The relative influence of the hemispherical caps becomes gradually less important with increasing L/D ratios and vanishes for spherocylinders with $L/D \to \infty$. The latter limit can be studied easily by computer simulation, because the partition function of spherocylinders in the limit $L/D \to \infty$ can be transformed to that of capless parallel cylinders of arbitrary length and diameter D. The phase behavior of parallel cylinders is independent of the value of L, because the latter merely fixes the length scale along the direction of the particle axes. We stress that this procedure is, of course, only valid when the particles are perfectly aligned.

The equation of state for hard parallel cylinders is displayed in Fig. 8. The data, which are also collected in Table VI, were obtained by performing MC simulations on a system of $N=90$ particles. We refer to Sec. II for the computational details of the simulations. The virial coefficients of the low-density nematic branch are

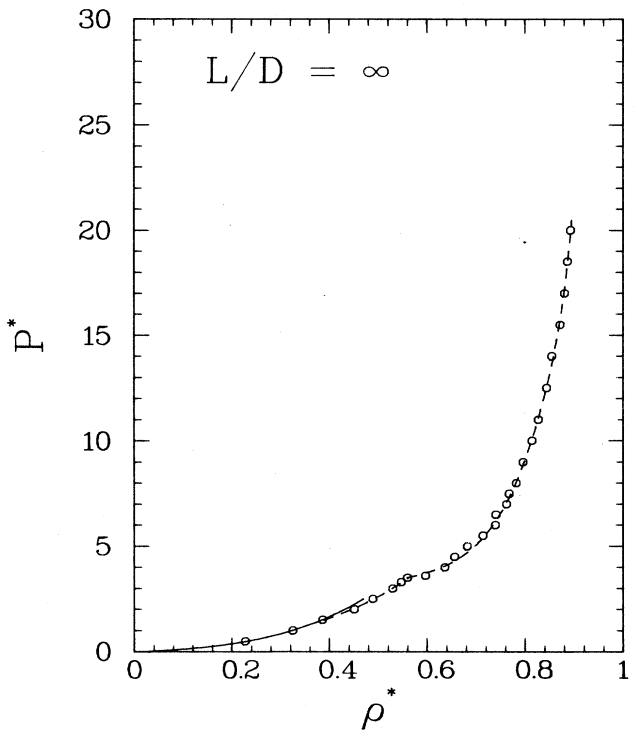

FIG. 8. Equation of state of hard parallel spherocylinders in the limit $L/D \to \infty$. Open circles, MC data; solid line, five-term virial series; dashed lines, fits through the MC data. Note the change of slope at $\rho^*=0.39$ and $\rho^*=0.56$, corresponding to a continuous nematic-smectic and a continuous smectic-columnar transition, respectively.

TABLE VI. Equation-of-state data for the nematic, smectic, and columnar phase of hard parallel spherocylinders in the limit $L/D \to \infty$. The density $\rho^* = \rho/\rho_{cp}$ and $P^* = Pv_0/kT$.

Nematic		Smectic		Columnar	
P^*	ρ^*	P^*	ρ^*	P^*	ρ^*
0.5	0.227	2.0	0.451	3.6	0.597
1.0	0.325	2.5	0.489	4.0	0.636
1.5	0.386	3.0	0.529	4.5	0.656
		3.1	0.534	5.0	0.682
		3.2	0.544	5.5	0.714
		3.3	0.547	6.0	0.739
		3.4	0.559	6.5	0.741
		3.5	0.560	7.0	0.762
				7.5	0.768
				8.0	0.782
				9.0	0.796
				10.0	0.814
				11.0	0.827
				12.5	0.844
				14.0	0.854
				15.5	0.871
				17.0	0.880
				18.5	0.887
				20.0	0.893

collected in Table III, whereas the coefficients of the y-expansion fits to the equation-of-state data are shown in the Table IV.

The phase behavior up to densities of approximately 50% of close packing is quite similar to the behavior of spherocylinders with $L/D \geq 0.5$. The hard-cylinder fluid apparently undergoes a continuous nematic-to-smectic transition at a density $\rho^* = 0.39$. The onset, at this point, of one-dimensional translational order along the particle axes results in a solidlike $g_{\parallel}(z)$ correlation function. Closer inspection of Fig. 8 shows that there is a cusp in the equation of state at $\rho^* = 0.56$. It appears that at this density the smectic phase transforms spontaneously into a columnar phase. The transition point can be traversed in both directions without any hysteresis effects. Furthermore, on both sides of the transition we observe strong pretransitional fluctuations. The presence of such fluctuations suggests that parallel cylinders undergo a continuous phase transition from the smectic to the columnar phase. We recall that the smectic-to-columnar transition is clearly first order in the case of spherocylinders with $L/D = 5$. For the $L/D \to \infty$ system we did not find a stable solid branch. This is not unexpected because, whereas a system of parallel spherocylinders at high densities can increase its entropy by transforming from the columnar to the crystalline phase, no such gain in entropy is possible for the parallel cylinders in the columnar phase.

The fact that the hard cylinder system undergoes apparently no first-order phase transition allows us to compare the two-dimensional Einstein crystal method for the free-energy computation of the columnar phase (Sec. III B) with a simple thermodynamic integration along the reversible path from the columnar phase to the ideal-gas reference state. The integration in Eq. (1) is performed by using the coefficients of the y-expansion fits in Table IV. The data pertaining to the Einstein crystal method are collected in Table V(b). Thermodynamic integration method:

$$\frac{F_N}{NkT}(\rho^* = 0.6962) = 3.265 .$$

Einstein crystal method:

$$\frac{F_N}{NkT}(\rho^* = 0.6962) = 3.733 .$$

The discrepancy between the results obtained by the two methods is surprisingly large. For comparison, thermodynamic integration and Einstein crystal method yield virtually indistinguishable results for the crystalline solid.[24] The reason for the discrepancy between the two techniques in the case of the columnar phase is, at present, not known. The most likely explanation appears to be that the peculiar shape of the capless cylinders makes it difficult to relax nonscalar stresses in the system.

E. The phase diagram

By combining the information on the various phase transitions presented in Secs. III A–III D we can construct the phase diagram of hard parallel spherocylinders as a function of the length-to-width ratio L/D. The densities at the observed continuous phase transitions are shown in Table VII(a). The densities of the coexisting phases as well as the pressure and the chemical potential at the transition are collected in Table VII(b). The phase diagram displayed in Fig. 9 shows the regions of thermodynamical stability of the nematic, smectic, columnar, and crystalline phases. In the limit $L/D \to 0$, the phase behavior follows from the data of Hoover and Ree[2] on hard spheres. The data pertaining to hard parallel cylinders [Table VII(c)] provide information about the behavior in the limit $L/D \to \infty$.

The most striking aspect of the phase diagram is the existence of thermodynamically stable smectic and columnar phases. This is, to our knowledge, the first time that liquid crystalline phases with partial translational order have been observed in a three-dimensional hard-core model system. The translational degrees of freedom of spherocylinders with $L/D > 3$ are actually frozen one by one, upon increasing the density from the translationally disordered nematic phase to the ordered crystalline phase.

The density at the melting point is initially quite comparable to that of the hard-sphere solid, but shifts gradually towards higher values for $L/D > 3$ when an additional columnar phase is formed between the smectic and the crystalline phase. The region of stability of the solid phase vanishes in the limit $L/D \to \infty$ where a three-dimensional crystalline structure is only formed at infinite pressure.

It appears that a small degree of nonsphericity, i.e., $L/D = 0.5$, is sufficient for a smectic phase to be thermodynamically stable. For the present model system, the nematic-smectic phase transition is apparently al-

TABLE VII. Density ρ^*, pressure P^*, and chemical potential μ^* at the phase transitions in a system of hard parallel spherocylinders with $L/D=0.25$, 0.5, 1, 2, 3, 5 [(a) and (b)] and in the limit $L/D\to\infty$ (c). (a) The continuous nematic-smectic transition as a function of L/D. (b) Coexistence points corresponding to the first-order smectic-columnar and columnar-solid phase transitions, as a function of L/D. (c) Density at the continuous nematic-smectic and the continuous smectic-columnar transitions in a system of hard parallel cylinders ($L/D\to\infty$).

L/D	ρ^*_{nem}	ρ^*_{smec}	ρ^*_{col}	ρ^*_{sol}	P^*	μ^*
		(a)				
0.25						
0.50		0.56			3.56	9.98
1.00		0.50			2.62	7.29
2.00		0.48			2.31	5.85
3.00		0.47			2.22	5.27
5.00		0.46			2.11	4.56
		(b)				
0.25	0.610			0.685	4.75	12.97
0.50		0.612		0.665	4.58	12.17
1.00		0.624		0.650	4.50	11.41
2.00		0.751		0.802	9.99	19.36
3.00		0.771		0.818	11.22	20.57
5.00		0.613	0.694		5.44	11.09
			0.892	0.911	25.90	38.93
		(c)				
$L/D\to\infty$	0.39				1.50	5.42
		0.56			3.50	9.48

ways continuous. The change in density, associated with the first-order transition from the smectic to the columnar phase for $L/D>3$, appears to be a decreasing function of the L/D ratio. In the limit $L/D\to\infty$, the smectic phase transforms continuously into the columnar phase without an observable density jump. Whether the smectic-columnar tricritical point is at $L/D=\infty$ or somewhere between $L/D=5$ and ∞ is not known at present.

The nematic-to-smectic transition density is only weakly L/D dependent and ranges from $\rho^*=0.50$ in the case of spherocylinders with $L/D=1$ to $\rho^*=0.39$ in the

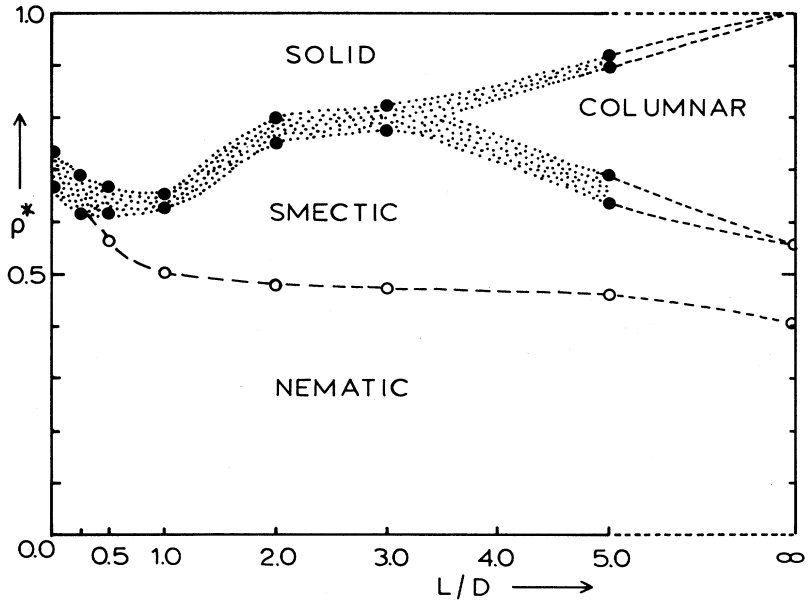

FIG. 9. Phase diagram of hard parallel spherocylinders, as a function of the length-to-width ratio L/D. The shaded areas correspond to two-phase regions. Black circles, densities of the coexisting phases; open circles, densities corresponding to the continuous nematic-smectic and smectic-columnar transitions. Note that the smectic-to-columnar transition appears continuous at $L/D\to\infty$. At present we do not know at what L/D value the transition looses its first-order nature.

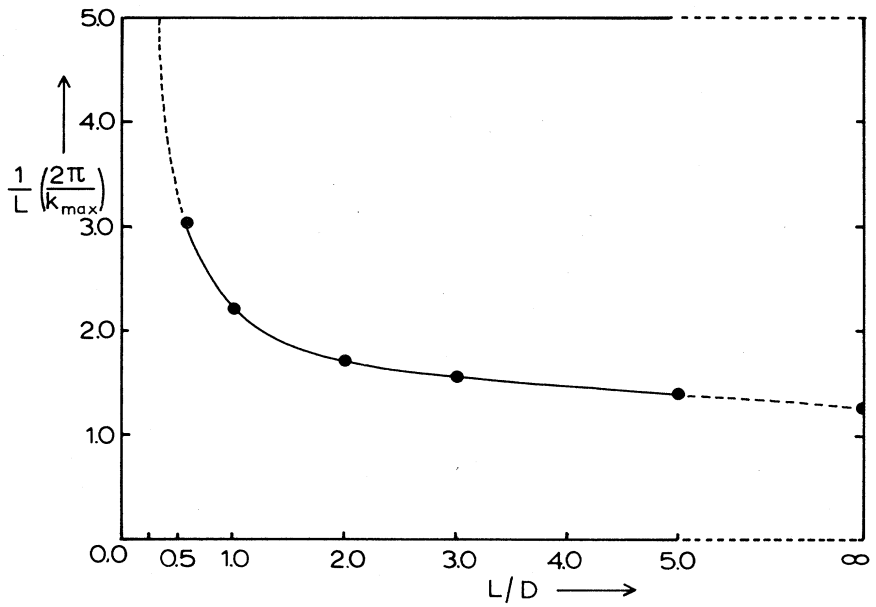

FIG. 10. L/D dependence of the periodicity $d=2\pi/k_{\max}$ of the smectic density wave at the nematic-smectic transition. The interlayer spacing is scaled with respect to the length L of the spherocylinder.

limit $L/D\to\infty$. For $L/D=0.50$, the transition moves to higher densities and we do not observe a smectic phase at all in the case of $L/D=0.25$. The L/D dependence of the smectic layer spacing at the nematic-smectic transition is shown in Fig. 10. The periodicity of the smectic density wave is mainly determined by the L/D ratio. The decrease of the interlayer spacing with density never exceeds 10% over the range of thermodynamical stability of the smectic phase. The nematic-smectic transition in a system of hard parallel cylinders has recently been investigated within the framework of a density-functional formalism.[26] The calculated transition parameters (a critical density $\rho^*=0.41$ and a smectic periodicity $d=1.34L$) are in surprising agreement with our results in the limit $L/D\to\infty$ ($\rho^*_{\rm MC}=0.39$; $d_{\rm MC}=1.27L$).

Summarizing, we conclude that our simple model system of hard parallel spherocylinders exhibits a particularly rich phase behavior. We recall that the phase behavior of hard parallel ellipsoids of revolution is independent of their eccentricity and hence similar to that of hard spheres. Nevertheless, the density-induced phase transitions in both hard-core systems are the result of a competition between the translational entropy and the entropy associated with the excluded volume effects. The latter are more subtle in the case of spherocylinders because the cylindrical segments fill space more efficiently than the hemispherical caps. The details of these excluded volume effects obviously play a crucial role in determining the phase behavior of anisometric hard-core particles.

One important factor that we have not discussed in this paper is the effect of orientational degrees of freedom on the phase diagram. We should expect that relaxing the requirement of parallel alignment will have a drastic effect on the phase diagram. In particular, we should expect a low-density isotropic phase. Moreover, the range of stability of all other phases is expected to change. It is, in principal, conceivable that the orientational freedom will completely destroy the smectic and columnar order. However, preliminary simulations on a system of nonaligned spherocylinders with $L/D=5$ indicate that at least in that system a stable smectic phase is still possible.[27] A systematic study of the phase diagram of freely rotating spherocylinders is currently under way.

ACKNOWLEDGMENTS

Computer time on the Amsterdam Cyber 205 was kindly made available by the University of Utrecht and Control Data Corporation.

[1]B. J. Alder and T. E. Wainwright, J. Chem. Phys. **27**, 1208 (1957).
[2]W. G. Hoover and F. H. Ree, J. Chem. Phys. **49**, 3609 (1968).
[3]J. A. Barker and D. Henderson, Rev. Mod. Phys. **48**, 587 (1976).
[4]M. Baus and J. L. Colot, Mol. Phys. **55**, 653 (1985).
[5]S. Hachisu and K. Takano, Adv. Colloid Interface Sci. **16**, 233 (1982).

[6]P. N. Pusey and W. van Megen, Nature **320**, 340 (1986).
[7]H. Zocher, Z. Anorg. Chem. **147**, 91 (1925).
[8]G. Oster, J. Gen. Physiol. **33**, 445 (1950).
[9]I. Langmuir, J. Chem. Phys. **6**, 873 (1938).
[10]L. Onsager, Ann. NY Acad. Sci. **51**, 627 (1949).
[11]R. Eppenga and D. Frenkel, Mol. Phys. **52**, 1303 (1984).
[12]D. Frenkel and B. M. Mulder, Mol. Phys. **55**, 1171 (1985).
[13]W. L. McMillan, Phys. Rev. A **4**, 1238 (1971).
[14]A. Kloczkowski and J. Stecki, Mol. Phys. **55**, 689 (1985).
[15]F. Dowell, Phys. Rev. A **28**, 3526 (1983).
[16]Y. Maeda and S. Hachisu, Colloids Surf. **6**, 1 (1983).
[17]M. Hosino, H. Nakano, and H. Kimura, J. Phys. Soc. Jpn. **46**, 1709 (1979).
[18]J. L. Lebowitz and W. J. Perram, Mol. Phys. **50**, 1207 (1983).
[19]W. W. Wood, J. Chem. Phys. **48**, 415 (1968).
[20]I. R. McDonald, Mol. Phys. **23**, 41 (1972).
[21]R. Najafabadi and S. Yip, Scr. Metall. **17**, 1199 (1983).
[22]F. H. Ree and W. G. Hoover, J. Chem. Phys. **40**, 939 (1964).
[23]B. Barboy and W. M. Gelbert, J. Chem. Phys. **71**, 3053 (1979).
[24]D. Frenkel and A. Ladd, J. Chem. Phys. **81**, 3188 (1984).
[25]L. Tonks, Phys. Rev. **50**, 955 (1936).
[26]B. M. Mulder, Phys. Rev. A **35**, 3095 (1987).
[27]D. Frenkel, J. Phys. Chem. (to be published).